DIFFRACTION AT HERA*

K. Hiller

for the H1 and ZEUS Collaborations

DESY Zeuthen, Platanenallee 6, D-15738 Zeuthen, Germany

(Received December 1, 2003)

Studies of diffractive events performed by the H1 and ZEUS Collaborations at the HERA *ep* collider are presented. The data of vector meson and photon production, inclusive deep inelastic scattering and hadronic final states with open charm and jets are confronted with the predictions of the resolved Pomeron and colour dipole models.

PACS numbers: 12.38.Qk, 12.40.–y, 13.60.–r

1. Introduction

The first hints of diffraction at HERA came up with the observation of the so-called "rapidity gap events" in *ep* deep inelastic scattering (DIS) [1]. About 10% of the events are characterized by a lack of hadronic particle production in the proton hemisphere. Events with such a topology can be attributed to the exchange of a colourless object between the interacting proton and the virtual photon.

In hadron–hadron scattering diffractive processes are well-described in the frame of Regge phenomenology by the exchange of the leading vacuum singularity — the Pomeron ($\mathbb{P}$) [2]. At higher energies the increase of the total cross section is attributed to this process [3]. However, no satisfactory relationship between the phenomenological Regge asymptotics and the gauge theory of strong interaction Quantum Chromodynamics (QCD) exists so far. Perturbative QCD successfully describes processes at hard scales, however the bulk of soft processes remains rather poorly understood.

The large kinematic range accessible at HERA allows to study the transition range from hard to nonperturbative soft diffractive processes. The point-like coupling of the virtual photons in diffractive deep inelastic scattering (DDIS) allows to probes the partonic structure of the exchange. The

* Presented at the XXXIII International Symposium on Multiparticle Dynamics, Kraków, Poland, September 5–11, 2003.

resulting parton density functions (PDFs) can be used to describe diffraction in a large variety of hard processes. The final goal of these studies is the understanding of diffraction in terms of QCD as the fundamental theory of strong interaction.

Over the last ten years the H1 and ZEUS experiments have analysed a large variety of soft and hard diffractive processes. This report tries to review the main results. It includes the production of vector mesons (VMs) and photons in deeply virtual Compton scattering (DVCS), the measurement of the diffractive structure function $F_2^{D(3)}$ and their interpretation in the frame of QCD-motivated models, and the confrontation of these models with open charm and jet final states. Detailed reports of these topics can be found in [4].

2. Kinematics

The generic graph of diffractive ep scattering is shown in Fig. 1. It is characterized by two distinct hadronic systems X and Y resulting from the dissociation of the virtual photon and the proton. Between both systems no colour flow occurs resulting in a gap of particle production.

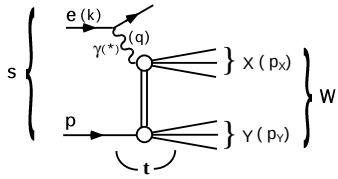

Fig. 1. The generic diffractive process $ep \to eXY$.

The standard DIS variables can be defined by the 4-vectors q and P of the incoming virtual photon and proton: the photon virtuality $Q^2 = -q^2$, the Bjorken variable $x = Q^2/2q \cdot P$, and the $\gamma^* p$ center of mass energy $W^2 = (q+P)^2$. For a complete description of the diffractive final state three additional variables are needed: the masses of the final states $M_X^2 = p_X^2$, $M_Y^2 = p_Y^2$, and the squared 4-momentum transfer $t = (P - p_Y)^2$, where p_X and p_Y are the 4-momenta of the outgoing systems X and Y, and t is the squared 4-momentum transfer between γ^* and p.

The kinematics of diffractive processes is usually expressed in terms of the variables:

$$x_{\mathbb{P}} = \frac{q \cdot (P - p_Y)}{q \cdot P} \approx \frac{M_X^2 + Q^2}{W^2 + Q^2}\,, \qquad \beta = \frac{Q^2}{2q \cdot (P - p_Y)} \approx \frac{Q^2}{M_X^2 + Q^2}$$

with $x_{\mathbb{P}}$ being the fractional momentum of the incoming proton transferred to X, and β can be interpreted as the fractional momentum of the quark coupling to the photon.

3. Selection methods

The absence of activity in the forward detectors is the main selection criterion of diffractive events. The system Y consist of the scattered proton or the products of the proton dissociation and escapes the central detector via the beam pipe. The most forward particle of system X defines the maximum pseudorapidity $\eta_{\max} = -\ln \tan(\theta/2)$, where θ is the polar angle of the outgoing hadron. The selection of diffractive events by an $\eta_{\max}$-cut limits $x_{\mathbb{P}}$ to the range $x_{\mathbb{P}} < 0.05$ with a contribution of about 15% p-dissociative events [5].

Another selection method is based on the direct measurement of the final state proton by forward proton spectrometers (FPSs). The FPS consists of movable tracking detectors along the beam line in distances up to 90 m from the interaction point [6]. The direct measurement of the scattered proton trajectory together with beam line optics can be used for the momentum reconstruction. In addition to the tracking detectors both HERA experiments use calorimeters to measure leading neutrons [7].

A third selection method is based on the measurement of the mass M_X of the virtual photon dissociation system. Diffractive processes prefer low M_X states with a shape $dN/dM_X^2 \propto 1/M_X^2$. Hence $dN/d\ln(M_X^2)$ is roughly constant and the diffractive events form a low M_X plateau. The amount D of diffractive events is the excess at small M_X above the exponential fall of the non-diffractive events parametrized by the ansatz: $dN/d\ln M_X^2 = D + c\exp(b\ln M_X^2)$ [8].

In case of VM production the diffractive events are identified through their charged decay particles without other hadronic activity in the central detectors. A large variety of VMs has been selected in this way: $\rho \to \pi^+\pi^-$, $\omega \to \pi^+\pi^-\pi^0$, $\phi \to K^+K^-$, $J/\Psi \to \mu^+\mu^-/e^+e^-$, and even smaller signals of ρ', $\Psi(2S)$, and Υ [9].

4. Vector meson and photon production

For different VMs the cross section in dependence on the γ^*p center of mass energy W is shown in Fig. 2. The measurements were performed at $Q^2 \approx 0$, integrated over the low t range and corrected for the fraction of proton dissociation [10]. It is clearly visible that the W dependence becomes steeper with increasing VM mass. The data are fitted by a Regge-motivated power law dependence W^δ and the resulting exponents increase from $\delta \approx 0.2$ for ρ up to $\delta \approx 1$ for $\Psi(2S)$. A large VM mass provides already in photoproduction a hard scale and the energy dependence of the cross section changes. The exponent δ can be related to the $\mathbb{P}$ intercept $\alpha_{\mathbb{P}}(0)$ by $\delta = 4(\alpha_{\mathbb{P}}(0) - 1 - \alpha'_{\mathbb{P}}/B)$, where $\alpha'_{\mathbb{P}}$ is the slope of the Pomeron trajectory and B the exponential slope of the t distribution.

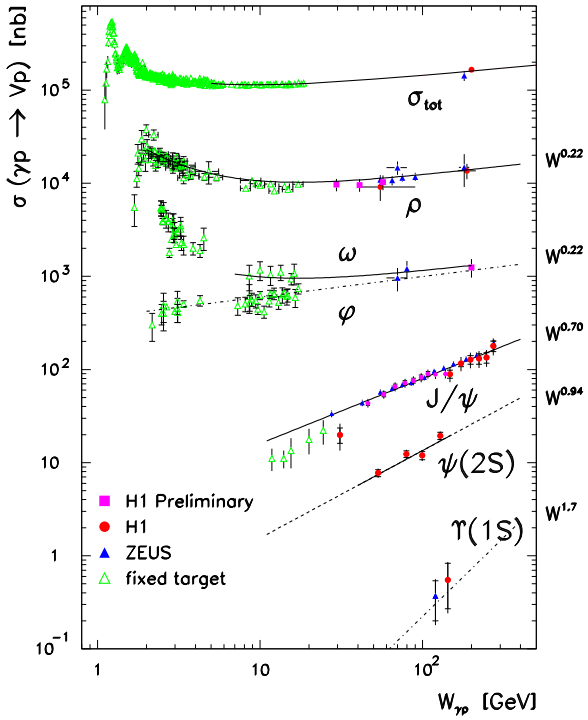

Fig. 2. Total and VM photoproduction cross sections parametrized by W^{δ}.

The SU(4) prediction for the VM cross sections ratios, neglecting mass differences and meson wave-functions, is: $\rho : \omega : \phi : J/\Psi = 9 : 1 : 2 : 8$. The measurements approach these values in the high Q^2 or t range [11]. The total elastic VM cross sections as a function of $(Q^2 + M_{\mathrm{V}}^2)$ scaled by the SU(4) factors are shown in Fig. 3. The values, except Υ [12], seem to follow a universal curve. This indicates the common underlying production mechanism at hard scales: a $q\bar{q}$ fluctuation of the virtual photon interacts perturbatively with the proton and condensates subsequently into a VM state [13].

The preferred scale to select perturbative processes is the high Q^2 range. The ρ meson cross sections at high Q^2 parametrized by W^{δ} is shown in Fig. 4 [14]. The exponent δ increases steadily up to $\delta \approx 1$ at highest Q^2, similar to that of J/Ψ photoproduction. The low t range of VM cross sections is well-described by the exponential form $\mathrm{e}^{-B|t|}$. The the exponent B decrease with increasing Q^2 or the VM mass [14]. This effect is related to the transverse size of the $q\bar{q}$ states which decrease with the mass or Q^2. In this picture the J/Ψ is already a small object in photoproduction, while the lighter ρ meson becomes small only at large Q^2.

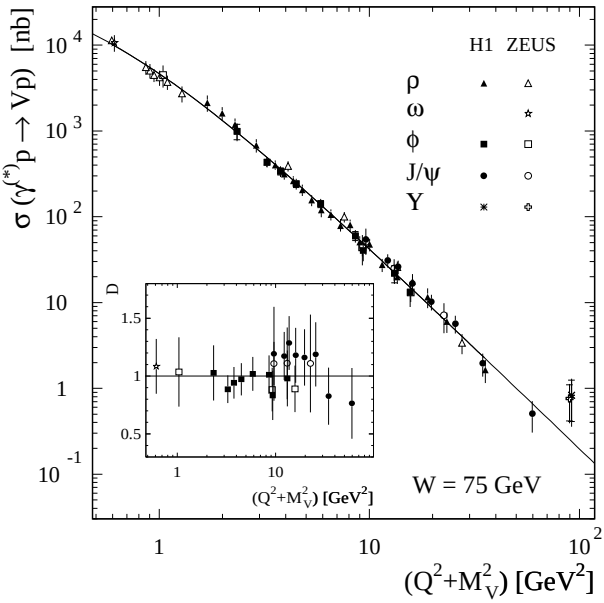

Fig. 3. The VM cross sections *versus* $Q^2 + M_V^2$ scaled by SU(4) factors.

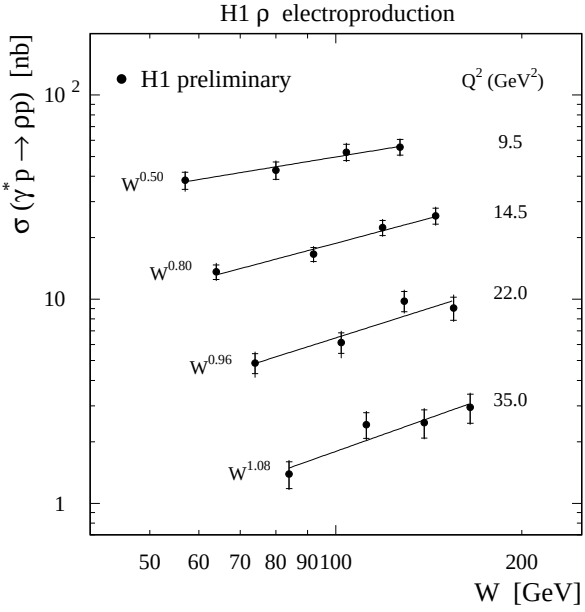

Fig. 4. The ρ cross section *versus* W for different Q^2 bins.

The high t range of ρ, ϕ and J/Ψ photoproduction is shown in Fig. 5 [15]. The BFKL calculation [16] gives for all three mesons a decent description, but also a power law dependence expected for a hard production mechanism is in good agreement with the data [17]. Hence, the large t range provides another hard scale to apply perturbative QCD calculations.

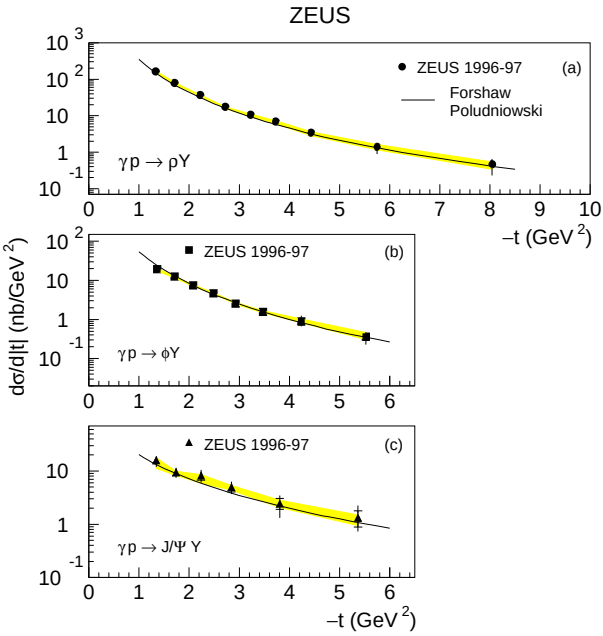

Fig. 5. The cross sections of ρ, ϕ, and J/Ψ *versus* t.

4.1. Deeply virtual Compton scattering (DVCS)

The DVCS process is similar to VM electroproduction, replacing the final state VM by a real photon. This allows QCD calculations without the theoretical complications related to the unknown VM wave function. The DVCS cross section factorizes into a hard scattering cross section calculable in perturbative QCD convoluted with the proton PDFs [18]. Another interesting aspect in DVCS is the potential to constrain generalized PDFs, which describe the correlation of partons in the proton [19].

The DVCS cross section measurements of H1 and ZEUS are combined in Fig. 6 [20]. The steep rise of the cross section, consistent with W^{δ}, $\delta \approx 1$, indicates the presence of a hard process and reflects the increase of the parton densities at smaller Bjorken x. The Q^2 dependence follows approximately a Q^{-3} behaviour.

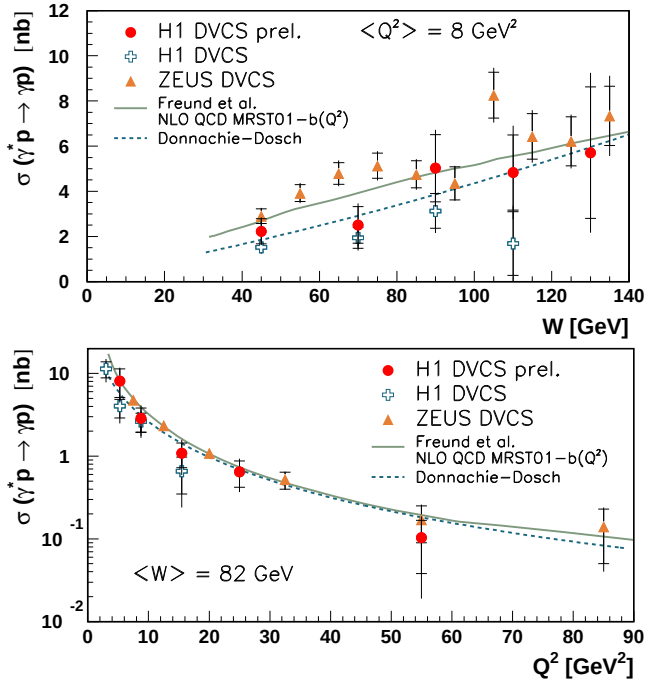

Fig. 6. The $\gamma^* p \to \gamma p$ cross section as a function of W and Q^2.

The measurements are compared to predictions of NLO QCD calculations using the MRST01 generalized PDFs [21] and a colour dipole model [22]. Both approaches contain soft and hard contributions and are in reasonable agreement with the data. Since the t distribution is unknown a slope $B = 7$ GeV^{-2} was assumed.

5. Diffractive deep inelastic scattering (DDIS)

At large Q^2 perturbative QCD has been successfully applied to describe inclusive DIS measurements [23]. In this context, the virtual photon can also be used to probe the structure of the diffractive exchange. The $ep \to eXY$ cross section is related to the reduced diffractive cross section and the diffractive structure functions by the following formulae:

$$\frac{d^3\sigma_{ep\to eXY}}{dx dQ^2 dx_{\mathbb{P}}} = \frac{4\pi\alpha_{\rm em}^2}{xQ^4}\left(1 - y + \frac{y^2}{2}\right)\sigma_r^{D(3)}(x, Q^2, x_{\mathbb{P}})\,,$$

$$\sigma_r^{D(3)}(x, Q^2, x_{\mathbb{P}}) = F_2^{D(3)} - \frac{y^2}{1 + (1-y)^2} F_{\rm L}^{D(3)}\,.$$

Since the outgoing proton system is not measured the structure functions are integrated over the low t range and corrected for the fraction of p-dissociation. The contribution of the longitudinal structure function $F_{\mathrm{L}}^{D(3)}$ is mostly below 1% and neglected.

5.1. The $x_{\mathbb{P}}$ dependence

The H1 measurement of $x_{\mathbb{P}}\sigma_r^{D(3)}$ in the low Q^2 range is shown in Fig. 7 [24]. The spectra are rather flat and no strong shape variations can be observed in the different bins of β and Q^2. Such a behaviour is consis-

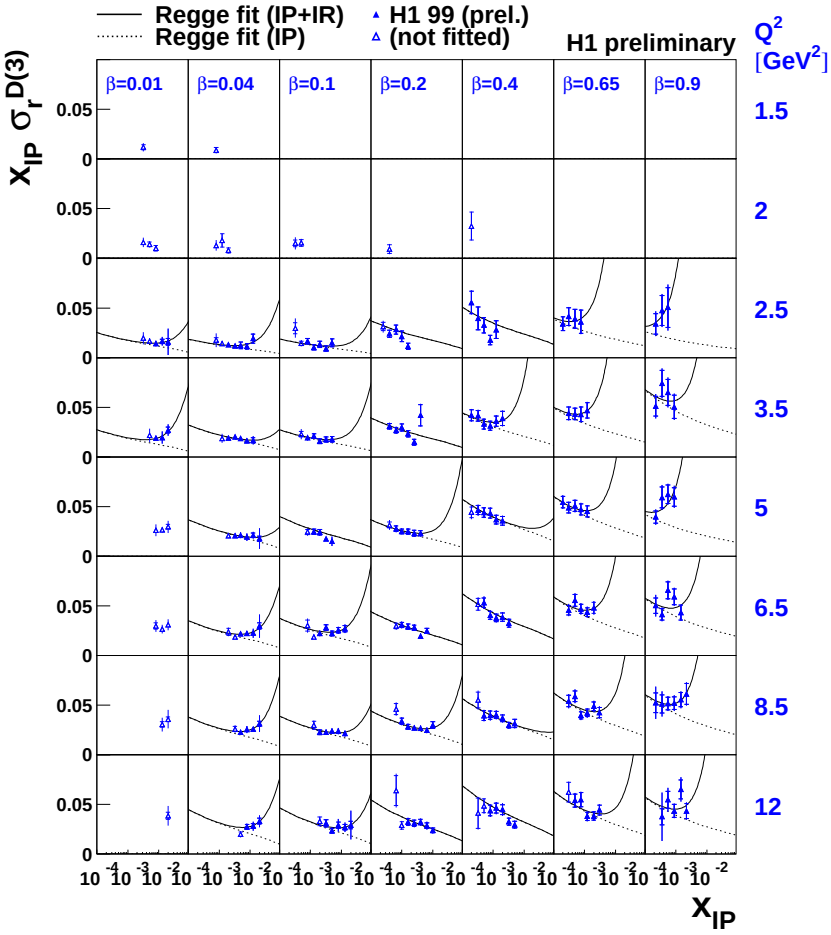

Fig. 7. The quantity $x_{\mathbb{P}}\sigma_r^{D(3)}$ *versus* $x_{\mathbb{P}}$ compared to a combined $\mathbb{P}$ and Regge fit. The dotted line indicates the $\mathbb{P}$ only contribution.

tent with the assumption of Regge factorization, which splits $\sigma_r^{D(3)}$ into $x_{\mathbb{P}}$ dependent $\mathbb{P}$ and subleading Reggeon ($\mathbb{R}$) flux factors and (β, Q^2)-dependent coefficients as shown in the following ansatz:

$$\sigma_r^{D(3)}(x_{\mathbb{P}}, \beta, Q^2) = f_{\mathbb{P}}(x_{\mathbb{P}}) A_{\mathbb{P}}(\beta, Q^2) + f_{\mathbb{R}}(x_{\mathbb{P}}) A_{\mathbb{R}}(\beta, Q^2)\,.$$

The fluxes are parametrized by the Regge-motivated ansatz: $f_{\mathbb{P},\mathbb{R}}(x_{\mathbb{P}}) \propto {x_{\mathbb{P}}}^{-2\bar{\alpha}_{\mathbb{P},\mathbb{R}}+1}$, where $\bar{\alpha}_{\mathbb{P},\mathbb{R}}$ are the values of the $\mathbb{P}$ and $\mathbb{R}$ trajectories averaged over the measured t range. In the fit procedure the $\mathbb{P}$ intercept $\alpha_{\mathbb{P}}(0)$ and the coefficients $A_{\mathbb{P},\mathbb{R}}(\beta, Q^2)$ are free parameters, the other Regge parameters and the t dependence were taken from hadronic measurements [25]. The fit results is shown in Fig. 7. The contribution of $\mathbb{R}$ exchange is clearly visible at large $x_{\mathbb{P}}$, while the $\mathbb{P}$ exchange dominates the range $x_{\mathbb{P}} < 0.01$.

In Fig. 8 the values of $\alpha_{\mathbb{P}}(0)$ obtained from the $x_{\mathbb{P}}$ dependence of the diffractive cross section in different regions of Q^2 are plotted. They are above the soft $\mathbb{P}$ value $\alpha_{\mathbb{P}}(0) \approx 1.08$ with the tendency to rise with increasing Q^2.

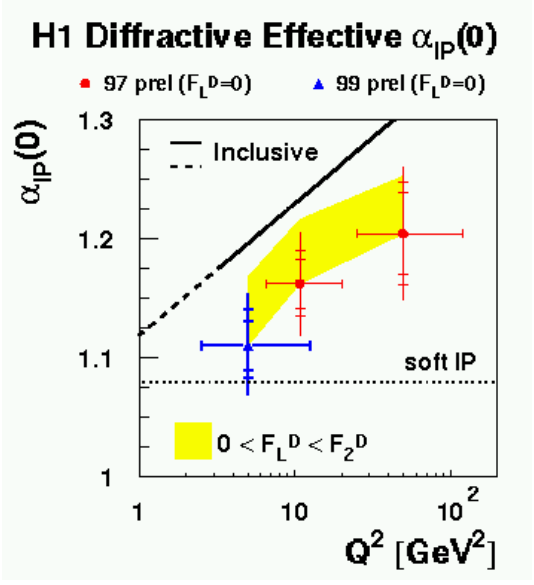

Fig. 8. $\alpha_{\mathbb{P}}(0)$ as a function of Q^2 obtained from the $x_{\mathbb{P}}$ dependence.

The ZEUS measurements of $\alpha_{\mathbb{P}}(0)$ are based on the W dependence of the diffractive cross section. The power law dependence $\sigma_{\text{diff}}^{\gamma^* p} \propto W^a$ was fitted to the cross sections in different M_X ranges. The exponent a is related to the Pomeron intercept by: $a = 4\bar{\alpha}_{\mathbb{P}} - 4$. In all M_X ranges except the low VM mass range a rise of $\alpha_{\mathbb{P}}(0)$ with Q^2 is observed [26].

5.2. Partonic interpretation of the Pomeron

The QCD factorization theorem allows the determination of diffractive PDFs from the DDIS measurements [27]. This theorem describes the reduced cross section $\sigma_r^{D(4)}(x_{\mathbb{P}}, t, x, Q^2)$ as the convolution of the perturbative QCD partonic cross section $\hat{\sigma}(x, Q^2)$ with diffractive PDFs $f^D(x_{\mathbb{P}}, t, x, Q^2)$.

The Q^2 dependence of the reduced cross section $\sigma_r^{D(3)}$ divided by the flux factors $f_{\mathbb{P}}$ in the range $x_{\mathbb{P}} < 0.01$ for different values of $x_{\mathbb{P}}$ in bins of β is shown in Fig. 9. The striking feature are the strong scaling violations up to high values of $\beta \approx 0.5$. Within the QCD evolution scheme such a behaviour results from a large gluon content of the diffractive exchange. In all Q^2 bins $\sigma_r^{D(3)}/f_{\mathbb{P}}$ is independent from $x_{\mathbb{P}}$ supporting the Regge factorization ansatz where the flux factor completely determines the $x_{\mathbb{P}}$ dependence. The QCD fit, also shown in Fig. 9, describes the Q^2 evolution quite well.

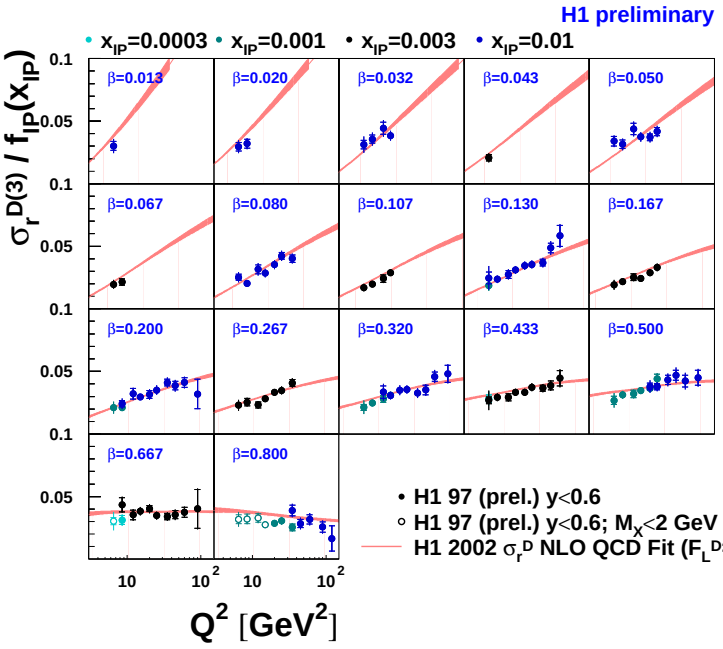

Fig. 9. The quantity $\sigma_r^{D(3)}/f_{\mathbb{P}}(x_{\mathbb{P}})$ *versus* Q^2 with the H1 NLO QCD fit.

Starting from a suitable ansatz for the quark and gluon densities at $Q_0^2 = 3$ GeV^2 the diffractive PDFs at higher Q^2 were obtained from the DGLAP evolution equations [28]. The resulting NLO quark singlet $\sum(z, Q^2)$ and gluon densities $g(z, Q^2)$ are shown in Fig. 10. Here the variable z corresponds to the fractional parton momentum of the diffractive exchange. The quark

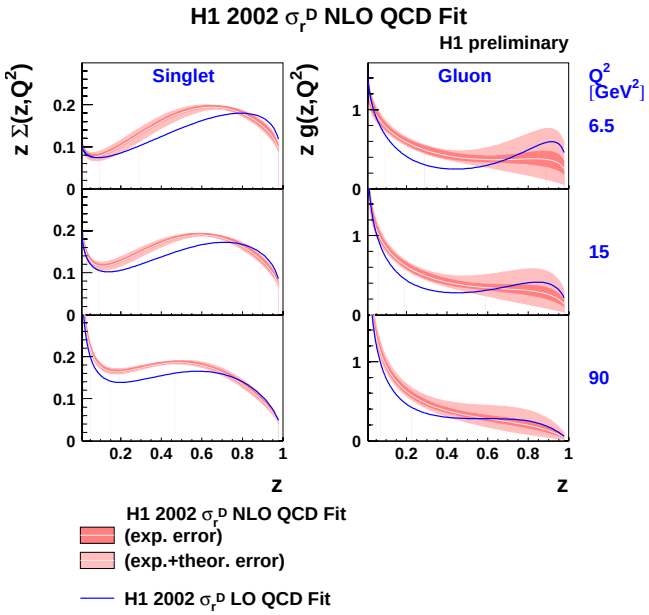

Fig. 10. The diffractive quark and gluon PDFs from the QCD fit.

and gluon PDFs extend up to large z, with a substantial uncertainty of the gluon PDF at $z > 0.5$. For all Q^2 the gluon dominates the momentum of the exchange consistent with a fraction of $75 \pm 15\%$.

The diffractive PDFs were obtained from fits to DDIS data in the range $6.5 < Q^2 < 120$ GeV^2. It is interesting to use these PDFs for extrapolations of cross sections outside the fitted range. The extrapolated cross section is in reasonable agreement with the measurements in the ranges $1.5 < Q^2 < 1600$ GeV^2 confirming the gluon dominance of the diffractive PDFs [29].

6. Forward baryon tagging

The use of the forward proton and neutron detectors completes the measurements of diffractive processes in several aspect:

1. the 4-momentum transfer t and so in principle the structure function $F_2^{D(4)}(x_{\mathbb{P}}, t, \beta, Q^2)$ can be measured,
2. no correction for the unknown fraction of p-dissociation are needed (the dominant systematic error of the untagged measurements),
3. the large overlap with non-diffractive range at lower p-momentum where the exchange of subleading Regge trajectories dominates.

Already the first measurements of forward baryon production at HERA have shown large contributions in the non-diffractive range $x_{\mathbb{P}} > 0.1$ [30]. In the angular range $\Theta < 0.8$ mrad, where Θ is the polar angle of the scattered proton, the ZEUS experiment has measured a fraction of 6.5% neutrons and 10% protons within $0.2 < x_{\mathrm{L}} < 1.0$ [1] and $0.6 < x_{\mathrm{L}} < 0.9$, respectively. While the proton fraction in the diffractive range $x_{\mathrm{L}} \to 1$ strongly increases the neutron contribution disappears.

The p_{T} dependence[2] of the diffractive cross section $\gamma^* p \to Xp$ was measured by ZEUS using the FPS in a large range of x_{L}, as shown in Fig. 11 [31]. All slope values are consistent with $b \approx 7$ GeV^{-2}.

Both HERA experiments have measured the structure functions with leading baryons. Fig. 12 shows the H1 result for a particular (x, Q^2) bin in the proton transverse momentum range $p_{\mathrm{T}} < 200$ MeV and $0.7 < x_{\mathrm{L}} < 0.9$ [32]. The data are reasonably well described by a Regge model including $\mathbb{P}$, $\mathbb{R}$ and π exchange. In the range $0.7 < x_{\mathrm{L}} < 0.9$ neutron production is compatible with π exchange whereas proton production requires all three contributions. As expected, the $\mathbb{P}$ contribution is small in the acceptance range but increases strongly for $x_{\mathrm{L}} \to 1$.

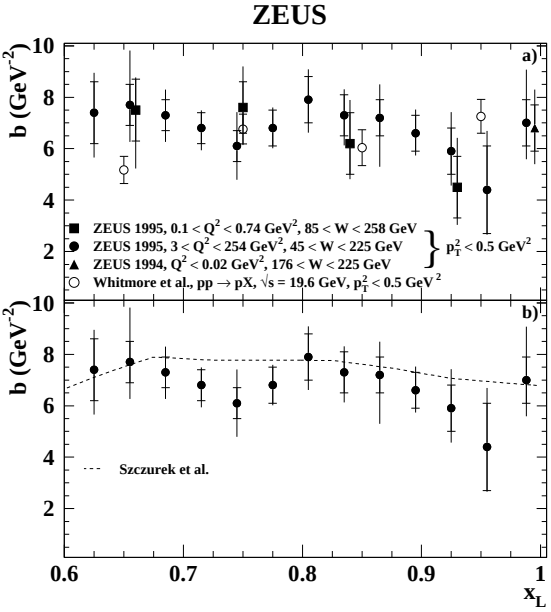

Fig. 11. The slopes b of the form $\mathrm{e}^{-bp_{\mathrm{T}}^2}$ as a function of x_{L} at different Q^2.

[1] $x_{\mathrm{L}} = 1 - x_{\mathbb{P}}$ is the fractional baryon momentum

[2] for $x_{\mathrm{L}} \approx 1$ in good approximation $t = -p_{\mathrm{T}}^2/x_{\mathrm{L}}$

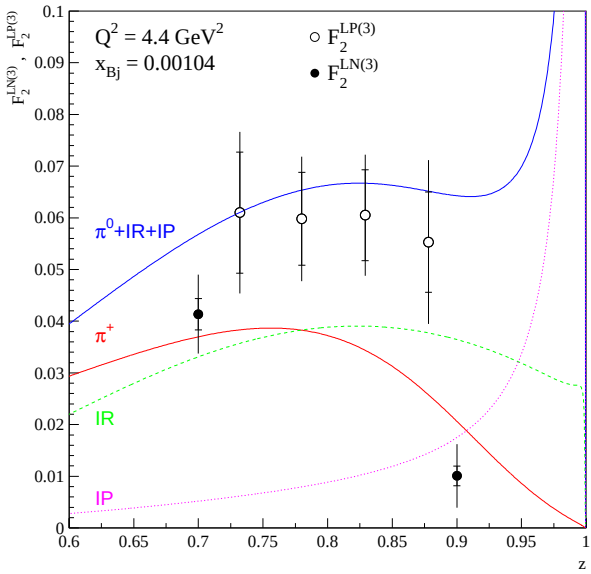

Fig. 12. The structure functions $F_2^{\mathrm{LP(3)},\mathrm{LN(3)}}$ as a function of the fractional baryon momentum.

7. Hadronic final states

Apart from the inclusive DDIS measurements many other diffractive processes are sensitive to the structure of the diffractive exchange. The diffractive PDFs obtained from the NLO QCD fit as well as other QCD models can be tested in more complex final states. From the analysis of DDIS processes in terms of colour dipole or the resolved Pomeron models one knows that the diffractive exchange is dominated by gluons. Hence processes which are mainly attributed to the boson–gluon fusion are an excellent test ground for QCD models. In the following we select as examples the open charm production and the dijet production which are mainly coming from boson–gluon fusion.

7.1. Open charm production

Both HERA collider experiments have measured diffractive $D^*(2010)$ production using the D^*–D^0 mass difference method [33]. Fig. 13 shows the $D^*(2010)$ cross section as a function of $x_{\mathbb{P}}$ compared to the predictions of three QCD models. The NLO predictions, based on diffractive PDFs parton densities obtained from combined fits to the inclusive DDIS and diffractive dijet photoproduction measurements at HERA (ACTW[34]), describe the cross section reasonable well in the whole $x_{\mathbb{P}}$ range.

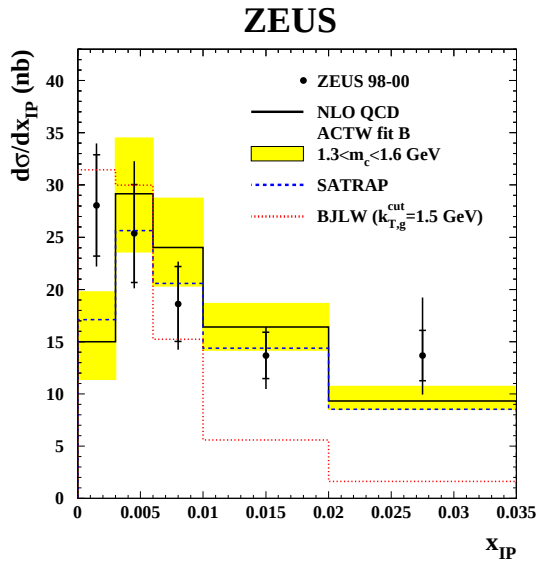

Fig. 13. The $D^{*\pm}$ cross section *versus* $x_{\mathbb{P}}$ compared with QCD models.

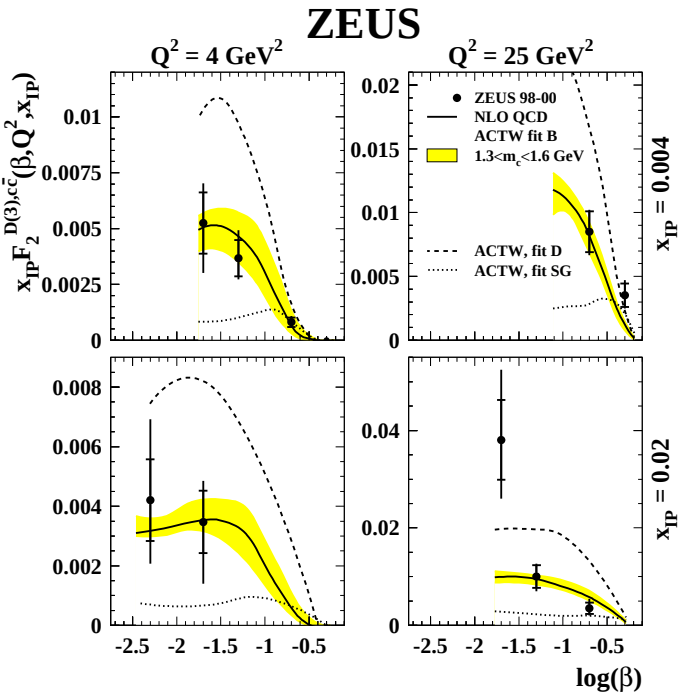

Fig. 14. $F_2^{D(3)c\bar{c}}$ *versus* β compared to different gluon-dominated PDFs.

In two other colour dipole models open-charm production is based on the virtual-photon fluctuation into $c\bar{c}$ and $c\bar{c}g$ states that interact with the proton via the exchange of gluon pairs. The saturation model SATRAP with k_{T}-ordering of the final state partons [35] agrees with the data whereas an alternative model of Bartels *et al.* BJWL [36] underestimates the charm cross section at $x_{\mathbb{P}} > 0.01$. With increasing statistics the charm data can also be used to constrain the gluon component of the diffractive exchange. Fig. 14 shows the charm structure function $F_2^{D(3)_{(c\bar{c})}}$ as a function of $\log(\beta)$ for different Q^2 and $x_{\mathbb{P}}$ values. The sensitivity of this measurement to different parametrizations of gluon-dominated PDFs is shown.

7.2. Dijet photoproduction

It has been demonstrated that jet production in hard processes can be described by QCD models using the diffractive PDFs obtained from the inclusive measurements [37]. The situation is more complex in photoproduction where additional resolved processes have to be taken into account. These processes resemble partonic interactions in hadron–hadron scattering different from the direct $\gamma^* q$ DIS scattering process.

The H1 experiment has analysed diffractive dijet photoproduction for an integrated luminocity of 18 pb^{-1} [38]. Events with transverse jet energies above 4 (5) GeV in the diffractive range $x_{\mathbb{P}} < 0.03$ were selected. The cross section in dependence on the fractional parton momenta $z_{\mathbb{P}}$ of the diffractive exchange and x_γ of the resolved photon is presented in Fig. 15. The data are compared to the resolved Pomeron model using gluon-dominated PDFs

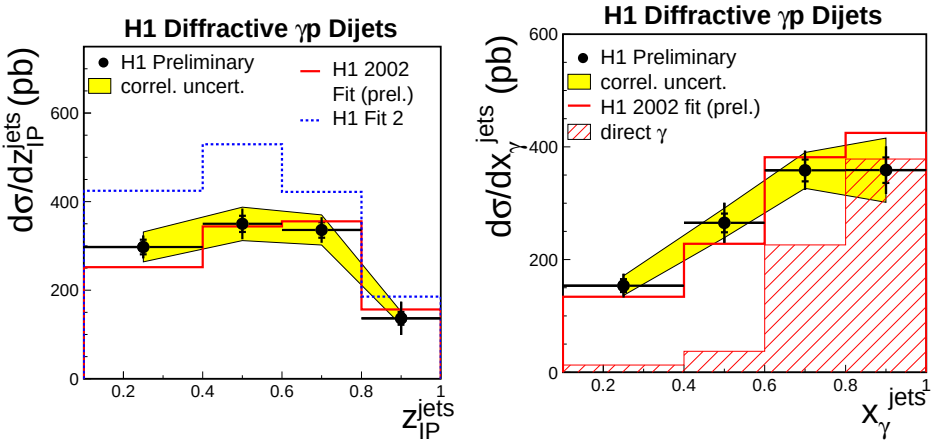

Fig. 15. The dijet cross section *versus* the fractional parton momenta $z_{\mathbb{P}}$ and x_γ of the underlying subprocess compared to the resolved Pomeron model.

for the diffractive exchange and the LO GRV photon PDFs [39]. While the recent DGLAP QCD fit [24] gives a good description of the $z_{\mathbb{P}}$ dependence an older set of PDFs [40] overestimates the normalization by a factor ≈ 1.4. As expected the dijet cross section in the range $x_\gamma > 0.6$ is dominated by the direct process. Adding the resolved contribution the model agrees with the data in shape and normalization.

8. Conclusions

The HERA *ep* collider is an ideal place to study diffraction in the transition region from soft to hard processes *versus* different scales like the VM mass, Q^2, t, E_{T} and others. It has been observed that the energy dependence of hard diffractive processes is steeper than those of soft processes. This change is directly related to the increase of the Pomeron intercept up to $\alpha_{\mathbb{P}}(0) \approx 1.2$ in the presence of a hard scale.

The DDIS data are compared with the predictions of two classes of QCD-motivated models: the resolved Pomeron and the colour dipole models. The latter models are based on the fluctuation of the virtual photon into $q\bar{q}$ or $q\bar{q}g$ colour dipoles and the subsequent interaction of the dipole with the proton.

The resolved Pomeron models factorize the diffractive process into three components: the flux of the diffractive exchange, its partonic structure and the cross section of the basic partonic subprocess. The DDIS data can be quite successfully fitted by the exchange of a hard Pomeron with a contribution of the subleading Reggeon in the range $x_{\mathbb{P}} > 0.01$. The main outcome of a NLO QCD fit using the DGLAP evolution scheme are the diffractive PDFs. In total, about 75% of the exchange momentum is carried by gluons and this gluon fraction remains large up to high β.

The comparison of QCD models with more complex hadronic final states can be used to test diffractive PDFs and the factorization ansatz. Due to the large gluon fraction of the exchange, final states with open charm or jets, produced mainly by boson–gluon processes, are the ideal test ground. Within the large error bands of these measurements the predictions of the QCD models agree with the data and confirm the gluon dominance of the exchange.

The results presented here are available thanks to the effort of many physicists in the H1 and ZEUS collaborations over nearly ten years of HERA running. I would like to thank the organizers for the opportunity to present these results at this stimulating conference.

REFERENCES

[1] (ZEUS Collaboration) M. Derrick *et al.*, *Phys. Lett.* **B315**, 481 (1993); (H1 Collaboration) T. Ahmed *et al.*, *Nucl. Phys.* **B429**, 477 (1994).

[2] P.D.B. Collins, *Introduction to Regge Theory and High Energy Physics*, Cambridge University Press, 1977.

[3] A. Donnachie, P.V. Landshoff, *Phys. Lett.* **B296**, 227 (1992).

[4] DIS2002 workshop, *Acta Phys. Pol. B* **33**, 2717 (2002).

[5] H1 Collaboration) C. Adloff *et al.*, *Z. Phys.* **C76**, 613 (1997).

[6] P. v. Esch *et al.*, *Nucl. Instrum. Methods Phys. Res.* **A446**, 409 (2000); (ZEUS Collaboration) M. Derrick *et al.*, *Z. Phys.* **C73**, 253 (1997).

[7] (H1 Collaboration) C. Adloff *et al.*, *Eur. Phys. J.* **C6**, 587 (1999); (ZEUS Collaboration) *Phys. Lett.* **B384**, 388 (1996).

[8] (ZEUS Collaboration) J. Breitweg *et al. Z. Phys.* **C75**, 3 (1997).

[9] (ZEUS Collaboration) J. Breitweg *et al. Eur. Phys. J.* **C14**, 213 (2000); (H1 Collaboration) A. Aktas *et al.*, *Phys. Lett.* **B568**, 205 (2003).

[10] (ZEUS Collaboration) J. Breitweg *et al.*, *Eur. Phys. J.* **C2**, 247 (1998); (H1 Collaboration) S. Aid *et al.*, *Nucl. Phys.* **B463**, 3 (1996); (ZEUS Collaboration) M. Derrick *et al.*, *Z. Phys.* **C73**, 73 (1996); (ZEUS Collaboration) J. Breitweg *et al.*, *Phys. Lett.* **B437**, 432 (1998); (ZEUS Collaboration) M. Derrick *et al.*, *Phys. Lett.* **B377**, 259 (1996); (H1 Collaboration) S. Aid *et al.*, *Nucl. Phys.* **B472**, 3 (1996); (ZEUS Collaboration) J. Breitweg *et al.*, *Z. Phys.* **C75**, 215 (1997).

[11] (ZEUS Collaboration) S. Chekanov *et al.*, *Eur. Phys. J.* **C26**, 389 (2003).

[12] (H1 Collaboration) C. Adloff *et al.*,*Phys. Lett.* **B483**, 360 (2000).

[13] L. Frankfurt *et al.*, *Phys. Rev.* **D54**, 3194 (1996); A. Martin *et al.*, *Phys. Rev.* **D55**, 4329 (1997); D. Ivanov, R. Kirschner, *Phys. Rev.* **D58**, 11402 (1998).

[14] (H1 Collaboration) X. Janssen, *Acta Phys. Pol. B* **33**, 3529 (2002).

[15] (ZEUS Collaboration) S. Chekanov *et al.*, DESY-02-072, submitted to *Eur. Phys. J.* **C**.

[16] J.R. Forshaw, G. Poludniowski, *Eur. Phys. J.* **C26**, 411 (2003).

[17] L. Frankfurt, M. Srikman, *Phys. Rev. Lett.* **63**, 1914 (1989); A.H. Mueller, W.K. Tang, *Phys. Lett.* **B284**, 123 (1992).

[18] A.V. Radyushkin, *Phys. Rev.* **D56**, 5524 (1999); J.C. Collins, A. Freund, *Phys. Rev.* **D59**, 074009 (1999); X. Ji, J. Osborne, *Phys. Rev.* **D58**, 094018 (1998).

[19] D. Mueller, D. Robaschik, B. Geyer, F.M. Dittes, J. Horejsi, *Fortschr. Phys.* **42**, 101 (1994); X. Ji, *Phys. Rev. Lett.* **78**, 610 (1997).

[20] (H1 Collaboration) C. Adloff *et al.*, *Phys. Lett.* **B517**, 47 (2001); (ZEUS Collaboration) S. Chekanov *et al.*, *Phys. Lett.* **B573**, 46 (2003).

[21] A. Freund, M. McDermott, *Eur. Phys. J.* **C23**, 651 (2002).

[22] A. Donnachie, H.G. Dosch, *Phys. Lett.* **B502**, 74 (2001).

[23] (H1 Collaboration) C. Adloff *et al.*, *Eur. Phys. J.* **C21**, 33 (2001).

[24] (H1 Collaboration) F. Schilling, contr. ICHEP2002, Amsterdam, 2002.

[25] (H1 Collaboration) C. Adloff *et al.*, *Z. Phys.* **C74**, 221 (1997).

[26] (ZEUS Collaboration) G. Wolf, contr. EPS2003, Aachen, 2003.

[27] J. Collins, *Phys. Rev.* **D57**, 3051 (1998), Erratum *Phys. Rev.* **D61**, 019902 (2000).

[28] V. Gribov, L. Lipatov, *Sov. J. Nucl. Phys.* **15**, 438 and 675 (1972); Y. Dokshitzer, *Sov. Phys. JETP* **46**, 641 (1977); G. Altarelli, G. Parisi, *Nucl. Phys.* **B126**, 298 (1977).

[29] (H1 Collaboration) F. Schilling, contr. EPS2003, Aachen, 2003.

[30] (ZEUS Collaboration) S. Chekanov *et al.*, *Nucl. Phys.* **B637**, 3 (2002).

[31] (ZEUS Collaboration) S. Chekanov *et al.*, *Nucl. Phys.* **B658**, 3 (2003).

[32] (H1 Collaboration) C. Adloff *et al.*, *Eur. Phys. J.* **C6**, 587 (1999).

[33] (H1 Collaboration) C. Adloff *et al.*, *Phys. Lett.* **B520**, 191 (2001); (ZEUS Collaboration) S. Chekanov *et al.*, DESY-03-115, 2003, submitted to *Phys. Rev.* **D**.

[34] L. Alvero *et al.*, *Phys. Rev.* **D59**, 074022 (1999).

[35] K. Golec-Biernat, M. Wuesthoff, *Phys. Rev.* **D59**, 014017 (1999).

[36] J. Bartels, H. Lotter, M. Wuesthoff, *Phys. Rev. Lett.* **B379**, 239 (1996); J. Bartels, H. Jung, A. Kyrieleis, *Eur. Phys. J.* **C24**, 555 (2002).

[37] (H1 Collaboration) C. Adloff *et al.*, *Eur. Phys. J.* **C20**, 29 (2001); (ZEUS Collaboration) S. Chekanov *et al.*,*Phys. Lett.* **B516**, 3 (2001).

[38] (H1 Collaboration) EPS03, Aachen 2003, abs.087, seesion 5.

[39] M. Glueck, E. Reya, A. Vogt, *Phys. Rev.* **D45**, 3986 (1992).

[40] (H1 Collaboration) C. Adloff *et al.*, *Z. Phys.* **C76**, 613 (1997).